

Near-Infrared Fluorescent Probe Activated by Nitroreductase for *In Vitro* and *In Vivo* Hypoxic Tumor Detection

Sanu Karan, Mi Young Cho, Hyunseung Lee, Hwunjae Lee, Hye Sun Park, Mahesh Sundararajan, Jonathan L. Sessler,* and Kwan Soo Hong*

Cite This: *J. Med. Chem.* 2021, 64, 2971–2981

Read Online

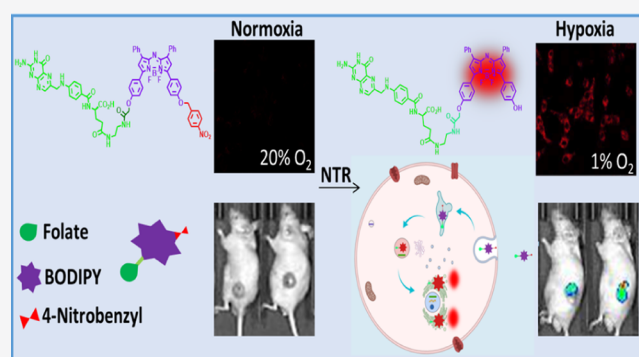
ACCESS |

Metrics & More

Article Recommendations

Supporting Information

ABSTRACT: Tumor hypoxia is correlated with increased resistance to chemotherapy and poor overall prognoses across a number of cancer types. We present here a cancer cell-selective and hypoxia-responsive probe (fol-BODIPY) designed on the basis of density functional theory (DFT)-optimized quantum chemical calculations. The fol-BODIPY probe was found to provide a rapid fluorescence “off–on” response to hypoxia relative to controls, which lack the folate or nitro-benzyl moieties. *In vitro* confocal microscopy and flow cytometry analyses, as well as *in vivo* near-infrared optical imaging of CT26 solid tumor-bearing mice, provided support for the contention that fol-BODIPY is more readily accepted by folate receptor-positive CT26 cancer cells and provides a superior fluorescence “off–on” signal under hypoxic conditions than the controls. Based on the findings of this study, we propose that fol-BODIPY may serve as a tumor-targeting, hypoxia-activatable probe that allows for direct cancer monitoring both *in vitro* and *in vivo*.



INTRODUCTION

Hypoxia is a common characteristic of solid tumor tissues, resulting from limited blood supply and inadequate oxygen delivery.¹ Various disease states are associated with chronic hypoxia, including cancer,^{2–5} intracellular infectious diseases,⁶ coronary and peripheral artery diseases,⁴ alcohol-induced liver injury,⁷ and gastrointestinal inflammatory conditions.^{8,9} Tumor hypoxia is correlated with treatment resistance, aggressive phenotypes, a large metastatic potential,¹⁰ and decreased overall survival rates.^{11,12} Therefore, it would be potentially beneficial to be able to detect and monitor hypoxia since doing so might allow therapies to be tailored to a particular status. It might also allow for tumor monitoring under conditions of clinical use, including surgical resection. Hitherto, several methods have been developed to detect hypoxia, such as blood flow velocity monitoring, oxygen electrodes, and methods based on hypoxia markers.¹³ However, given their ease of potential use, specific probes for hypoxic tumors could prove complementary to these existing methods. More generally, there is a need for cancer detection probes.^{14–16} Unfortunately, in many instances, the probes suffer from poor sensitivity. In the specific case of hypoxia probes, drawbacks include poor penetration, high scattering of the excitation and emission light through the tissues, and limits in the increase of fluorescence intensity seen in animal or clinical studies.¹⁷ Here, we report a conjugate (fol-BODIPY) that acts as a near-infrared (NIR) fluorescent hypoxia-sensitive probe and which operates in a

biologically convenient spectral region ($\lambda_{ex}/\lambda_{em} = 685/730$ nm).

Tumor hypoxia is correlated with increased levels of various enzymes, such as nitroreductase (NTR), azo-reductase, and quinonoreductase.^{18,19} Not surprisingly, therefore, many hypoxia-responsive probes have been conjugated to nitro, azo, selenium, and quinone moieties, which are sensitive to hypoxic microenvironments.^{20–23} Nevertheless, probes that may be used to image both intracellular hypoxia and hypoxia *in vivo* remain all but unknown. Alternative approaches to hypoxia sensing, including positron emission tomography and various ¹⁸F-labeled radiotracer-based strategies, have been reported; however, they too are plagued by major challenges, such as high background noise and limited spatial resolution.^{24,25}

In an effort to overcome some of the drawbacks associated with optical probes for *in vivo* cancer detection, increasing attention is being devoted to exploring the use of NIR fluorophores (i.e., agents with emission wavelengths above 700 nm).²⁵ To date, several hypoxia-sensitive NIR fluorophores

Received: December 15, 2020

Published: March 12, 2021



Scheme 1. Chemical Structures of fol-BODIPY and Controls 1 and 2 and Schematic Representation of Cancer Targeting and the Active Switching on of Fluorescence Expected under Hypoxic Conditions

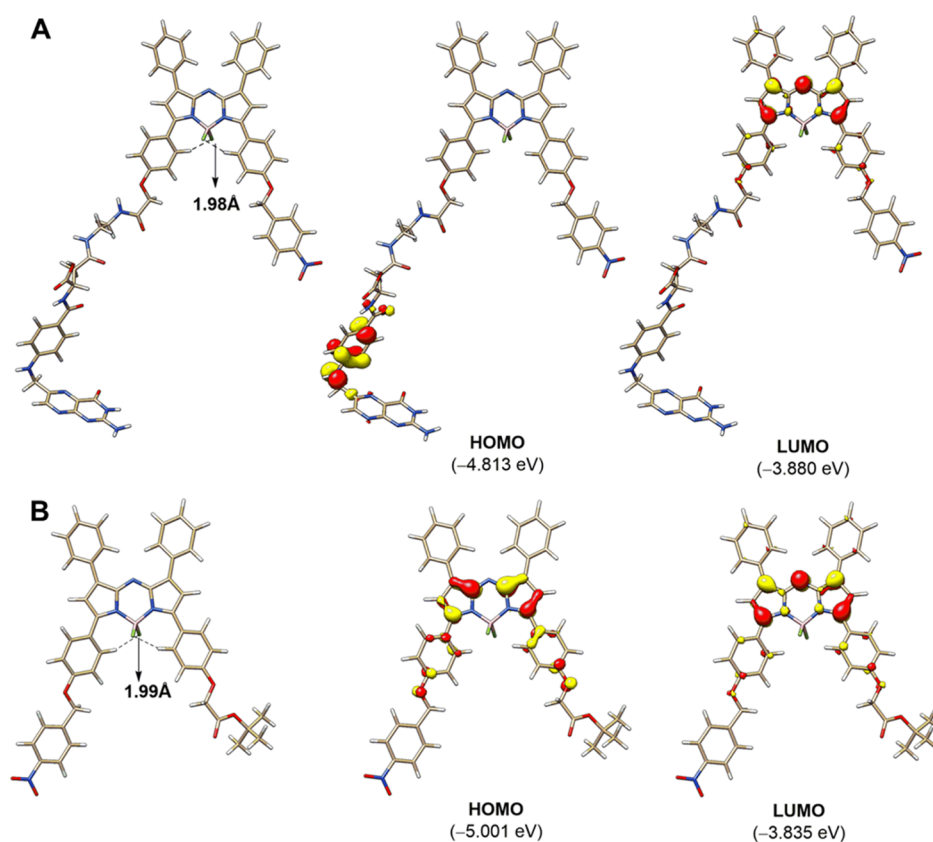
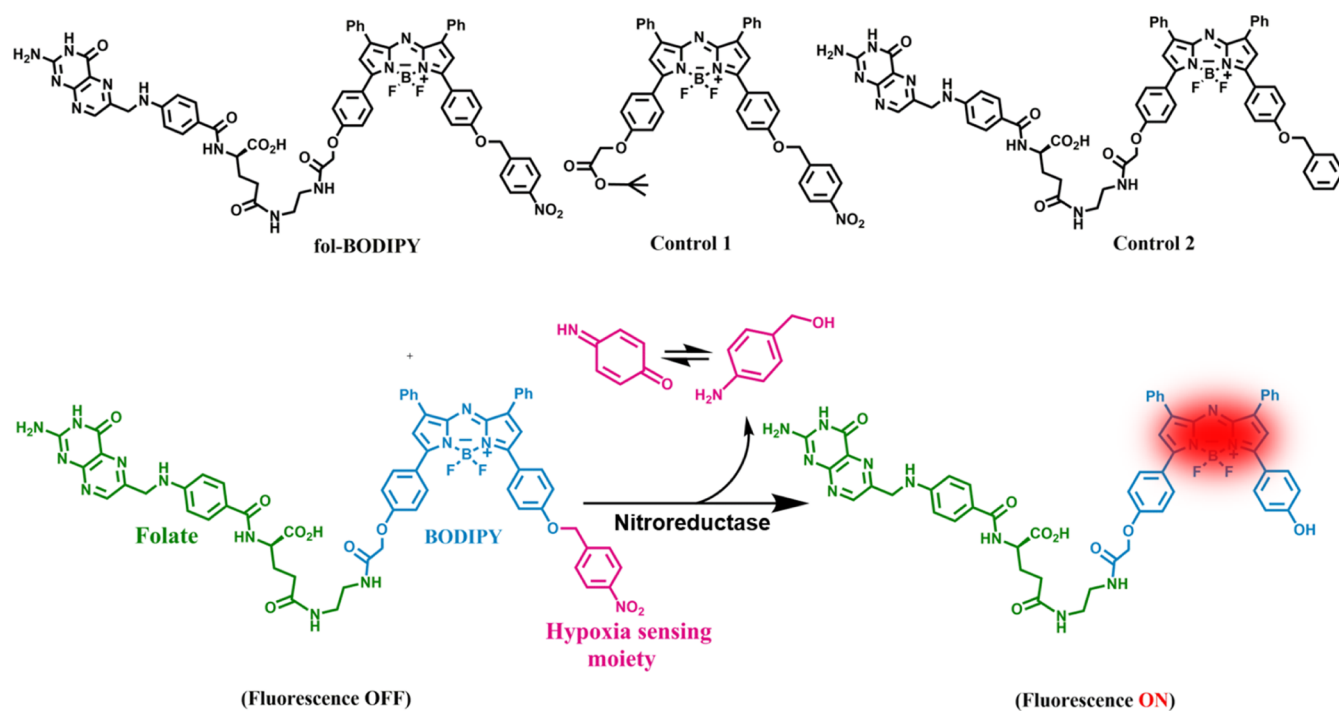


Figure 1. DFT-optimized structures, computed HOMO, and LUMO gaps for fol-BODIPY (A) and control 1 (B). The calculated energy gap for fol-BODIPY is $\Delta E_{\text{fol-BODIPY}} = (\text{HOMO} - \text{LUMO}) = -0.933$ eV, while that for the control 1 is -1.166 eV.

have been reported;^{26–31} however, few of these fluorophores possess a cancer-targeting moiety.^{32,33} Furthermore, few of these fluorophores can differentiate between normal and

cancer cells. Therefore, there remains a need for a tumor-targeting, hypoxia-responsive NIR probe that emits in the >700 nm spectral region.

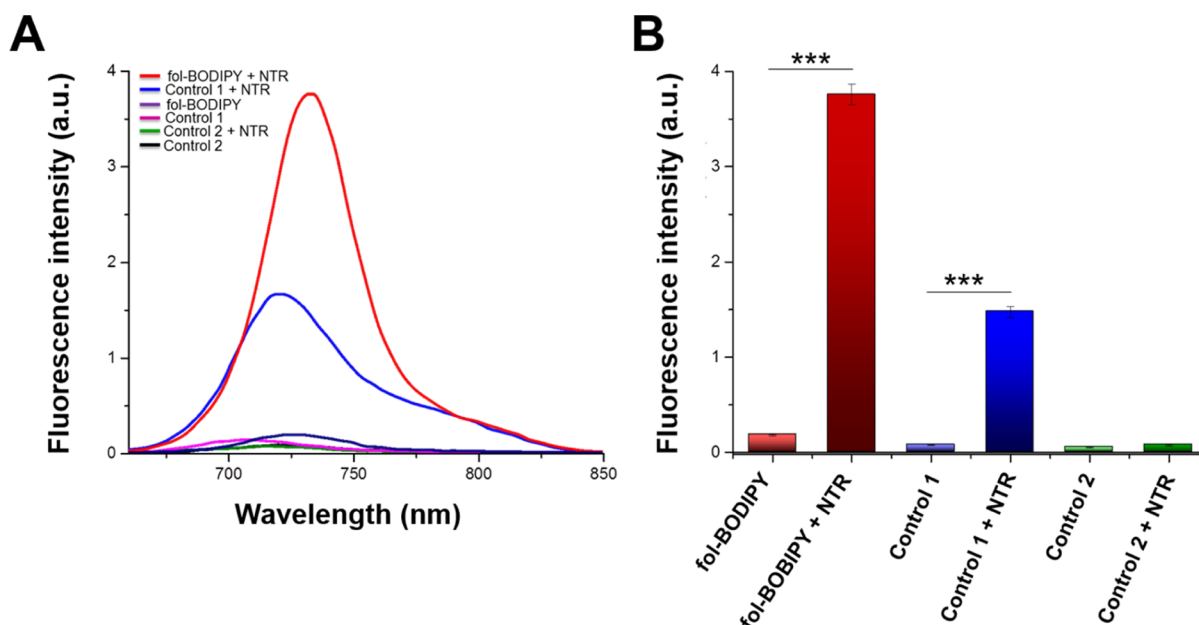


Figure 2. (A) Normalized fluorescence spectra of **fol-BODIPY**, control 1, and control 2 in the presence and absence of NTR (1 $\mu\text{g}/\text{mL}$) and (B) corresponding quantitative comparison of the fluorescence intensity. All experiments were carried out in the presence of NADH hydrate (200 μM). The data shown are the average of four independent experiments; error bars are the standard deviation (nonpaired Student's *t*-test). ****p* < 0.001.

BF_2 -chelated azadipyromethane class 1 ($\lambda_{\text{ex}} = 685 \text{ nm}$, $\lambda_{\text{em}} = 730 \text{ nm}$) probes (Scheme S1) are modified versions of BODIPY ($\lambda_{\text{ex}} = 493 \text{ nm}$, $\lambda_{\text{em}} = 503 \text{ nm}$), where class 1 refers to the nature and position of the pyrrole ring substitution (e.g., Ph at positions 3 and 5). These derivatives typically display good chemical stability in aqueous media, possess high fluorescence quantum yields, and are characterized by excellent photo-stability at an absorption/emission λ_{max} of 696/727 nm.^{34,35} Thus, to create a highly sensitive fluorescent off/on probe for hypoxic regions with cancer-targeting specificity, we aimed to build off a BF_2 -chelated azadipyromethane core, a class 1 probe known for its excellent photo-physical properties, high fluorescence quantum yield (0.3–0.4), and good photo-stability.^{36,37} As detailed below, this core was conjugated to a folate subunit to produce a conjugate (**fol-BODIPY**) that acts as an NIR fluorescent hypoxia-sensitive probe ($\lambda_{\text{ex}}/\lambda_{\text{em}} = 685/730 \text{ nm}$). The alpha isoform of the folate receptor (FR- α) is common in about 40% of human cancers and is especially prevalent in malignant tissues such as ovarian and colorectal cancers. This makes folate a useful cancer-targeting group. In contrast, folic acid or its conjugates do not accumulate appreciably in normal tissues.^{38–41} Not surprisingly, therefore, a range of folate-conjugated drugs and imaging agents have been developed recently.^{42–46}

The **fol-BODIPY** probe also contains a *p*-nitrobenzyl ether linkage. This is a known NTR cleavable trigger.⁴⁷ In the case of **fol-BODIPY**, it permits the selective targeting of hypoxic cancer cells overexpressing NTR *in vitro*, as well as hypoxic tumors *in vivo* as demonstrated using a xenograft mouse model.

RESULTS AND DISCUSSION

Design and Synthesis of fol-BODIPY. Our goal was to generate an efficient fluorescent probe that would allow for *in vivo* hypoxic tumor detection. We felt that such a putative probe would need to fulfill several specific requirements, including having an NIR optical window while displaying enhanced fluorescence with excellent sensitivity and selectivity.

With such design attributes in mind, a BF_2 -chelated azadipyromethane NIR probe was conjugated to an NTR-responsive *p*-nitrobenzyl moiety via a phenolic ether linker giving the **fol-BODIPY** probe (Scheme 1). This probe was synthesized in three successive steps as shown in Scheme S1. Precursors and mono-*O*-^tBu-BODIPY were synthesized in accordance with reported methods.^{48,49} Control 1 (Scheme S1) was formed by reacting mono-*O*-^tBu-BODIPY with 4-nitrobenzyl bromide with a yield of 78.3%. Compound **6a**, produced by deprotection of the BOC group in control 1 using trifluoroacetic acid, was reacted with *N*-hydroxysuccinimide in the presence of diisopropylethylamine to form a reactive intermediate (*N*-hydroxysuccinimide ester). This intermediate was subsequently reacted with folate ethylenediamine⁵⁰ to produce **fol-BODIPY** (Scheme S1). Control 2 was prepared using the same method but starting with compound **4** and benzyl bromide. The **fol-BODIPY** conjugate and controls 1 and 2 were characterized by ¹H and ¹³C NMR spectroscopy, as well as by HRMS (Figures S1–S18) and high-performance liquid chromatography (HPLC) analysis (Figure S19).

Figure 1 shows the density functional theory (DFT)-optimized structures and the frontier molecular orbitals expected to define the optical properties of **fol-BODIPY** (A) as well as those of control 1 (B). In both species, a presumed hydrogen bonding interaction between the $-\text{BF}_2$ group and the phenyl ring is inferred based on their proximity (ca. 1.99 Å). The computed energy gaps between the highest occupied molecular orbital (HOMO) and the lowest unoccupied molecular orbital (LUMO) between **fol-BODIPY** and control 1 are 0.93 and 1.17 eV, respectively. This leads us to suggest that **fol-BODIPY** will be more reactive and sensitive than its congener control 1. Based on this DFT-optimized structure, **fol-BODIPY** was selected for further study as a potential hypoxia probe. We then optimized the structure of the reduced aniline (but uncleaved) form of **fol-BODIPY** using a protocol analogous to that used in our previous studies^{51–53} (Figure S20A). We also computed the absorption spectrum of control

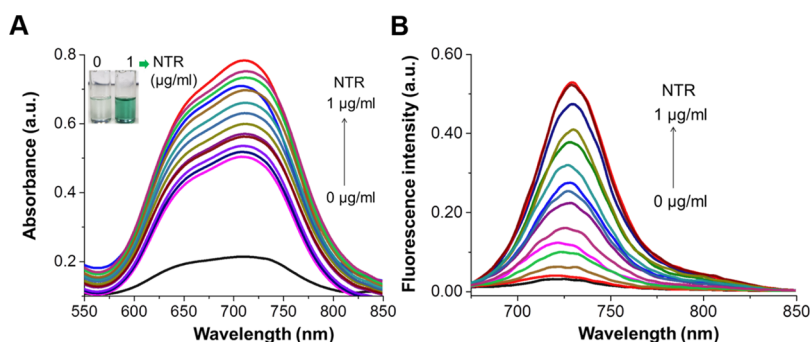


Figure 3. (A) UV absorption and (B) fluorescence emission ($\lambda_{\text{ex}} = 642 \text{ nm}$) spectra of fol-BODIPY ($5 \mu\text{M}$) recorded in the presence of various concentrations of NTR (0–1 $\mu\text{g/mL}$). All data points were acquired 30 min after the addition of NTR into the medium at $37 \text{ }^\circ\text{C}$.

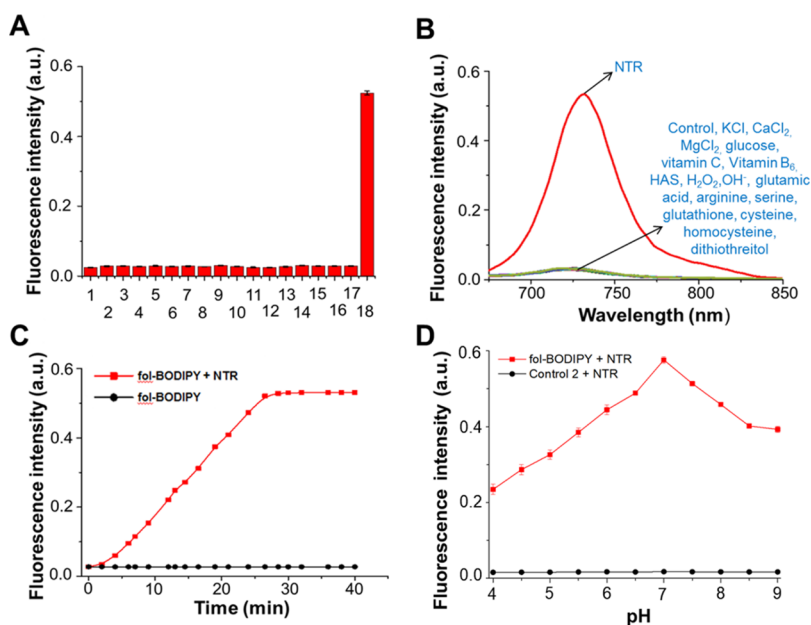


Figure 4. Fluorescence response of fol-BODIPY ($5 \mu\text{M}$) in the presence of NADH ($50 \mu\text{M}$) to various species (A): (1) fol-BODIPY + NADH, (2) 150 mM KCl, (3) 2.5 mM CaCl_2 , (4) 2.5 mM MgCl_2 , (5) 10 mM glucose, (6) 1 mM vitamin C, (7) 1 mM vitamin B_6 , (8) 100 μM HSA, (9) 10 μM H_2O_2 , (10) 10 μM $\cdot\text{OH}$, (11) 1 mM glutamic acid, (12) 1 mM arginine, (13) 1 mM serine, (14) 5 mM glutathione, (15) 1 mM cysteine, (16) 1 mM homocysteine, (17) 1 mM dithiothreitol (DTT), and (18) 0.5 $\mu\text{g/mL}$ NTR. (B) Fluorescence response at $\lambda_{\text{em}} = 730 \text{ nm}$ of fol-BODIPY ($5 \mu\text{M}$) with different species present in blood serum (graphically). (C) Time-dependent fluorescence intensity change of the probe ($5 \mu\text{M}$) in the presence of NTR (0.5 $\mu\text{g/mL}$). (D) Maximum fluorescence intensity increase seen when the fol-BODIPY probe ($5 \mu\text{M}$) is treated with NTR at different pHs per the conditions of (A). All experiments were carried out in the presence of NADH ($200 \mu\text{M}$) and an excitation wavelength (λ_{ex}) of 642 nm was used in all cases.

I using a range-separated DFT (CAM-B3LYP) in conjunction with the def2-SV(P) basis set as implemented in the ORCA package. We used 10 roots to predict the spectrum. The computed spectrum qualitatively matches the experimental data, as shown in Figure S20B. To gain further insights into the guiding structure–function relationships, we likewise carried out DFT calculations to understand the nature of Frontier orbitals that dictate the origin of absorption/emission spectrum of fol-BODIPY and control 1. The HOMO–LUMO gap of fol-BODIPY (0.933 eV) is smaller by 0.23 eV compared to those of control 1 (1.167 eV), leading us to infer that the former is more reactive than control 1.

Optical Properties of Fol-BODIPY. Based on considerable literature precedent,⁴⁷ it was expected that NTR would promote cleavage of the phenolic ether (–O–) bond in fol-BODIPY so as to release the active fluorophore. To test this hypothesis, fol-BODIPY and control 2 were treated with 1 $\mu\text{g/mL}$ NTR in the presence of nicotinamide adenine dinucleotide

(NADH) under physiological conditions (pH 7.4). The optical changes, if any, were then monitored using UV–vis and fluorescence spectroscopies (Figures S21–S22). Although no significant changes were observed for control 2 or in the absence of NTR, a remarkable enhancement in the fluorescence intensity at 730 nm was observed for fol-BODIPY in the presence of NTR (Figure 2). Such findings are consistent with the design expectation that NTR promotes reduction of the electron-withdrawing nitro group (–NO₂) to the corresponding electron-donating amine group (–NH₂), which then leads to self-immolative ether cleavage. The net result is release of the free fluorophore and a readily discernible enhancement in the fluorescence intensity. Since control 2 lacks a 4-nitro group, it and its associated optical features remain unchanged in the presence of NTR.

Figure 3 shows that the absorption maxima at 685 nm and the emission maxima at 730 nm increase steadily upon addition of NTR. The results presented in Figure 3A reveal

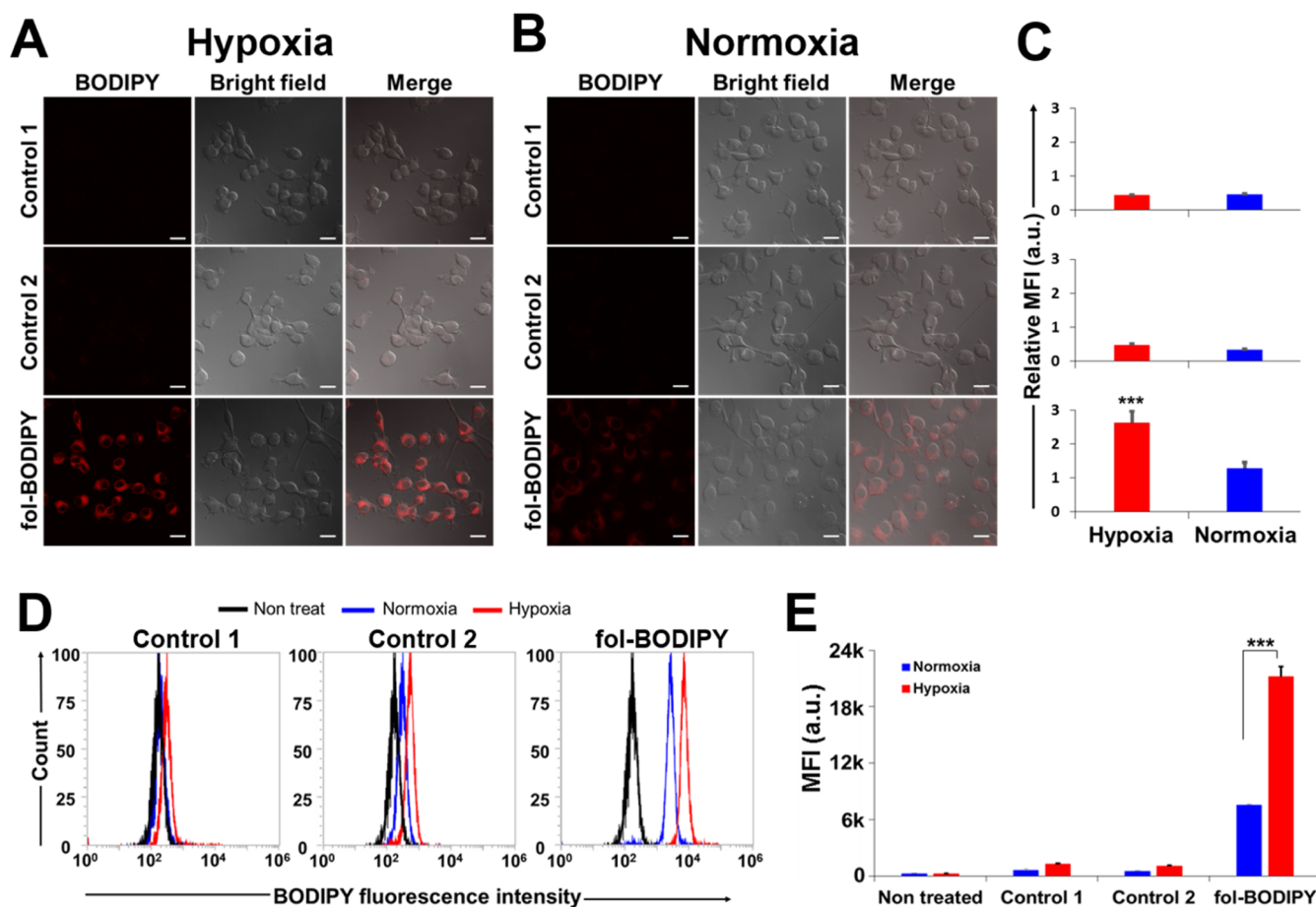


Figure 5. *In vitro* fluorescence imaging of CT26 cells. Representative confocal laser scanning microscopy (CLSM) images of CT26 cells incubated with fol-BODIPY or controls 1 and 2 (5 μM each) for 15 min under hypoxic (A) and normoxic (B) conditions. Scale bar, 20 μm . Images were obtained using an excitation wavelength of 633 nm and emission wavelengths in the 638–737 nm spectral region. (C) Corresponding quantitative hypoxia–normoxia ratio for control 1, control 2, and fol-BODIPY. Relative fluorescent intensity was measured from seven individual cells using ImageJ software (nonpaired Student's *t*-test). (D) FACS analyses of CT26 cells treated with fol-BODIPY and controls 1 and 2. Cells, incubated with PBS under hypoxic or normoxic conditions for 24 h, were treated with fol-BODIPY or controls 1 and 2 (5 μM each) for 15 min before flow cytometry analysis. (E) Comparison of the MFI measured using flow cytometry. Plotted data are the average of three independent experiments; error bars are the standard deviations (nonpaired Student's *t*-test). ****p* < 0.001.

that the intensity of the UV–vis absorption spectral feature centered at 685 nm in the case of fol-BODIPY gradually increases as a function of NTR concentration (0–1 $\mu\text{g}/\text{mL}$) up an apparent 8-fold maximum in the presence of 1 $\mu\text{g}/\text{mL}$ NTR. Similarly, the fluorescence intensity of fol-BODIPY was seen to increase ~ 20 -fold upon the addition of 1 $\mu\text{g}/\text{mL}$ NTR (Figure 3B). Based on a regression analysis, the calculated detection limit of the fol-BODIPY probe toward NTR was found to be 1.52 ng/mL (Figure S23). This represents a lower detection limit than that seen for previously reported probes^{22–29} and is equivalent to an ultrasensitive probe.²⁷

To gain further insights into the NTR-mediated release of an active fluorophore from fol-BODIPY, it was treated with 1 $\mu\text{g}/\text{mL}$ NTR in phosphate-buffered saline (PBS) for 1 h in the presence of NADPH. An aliquot was subjected to HR-MS analysis, which revealed inter alia two major peaks, one ascribable to the *p*-nitrobenzyl ether-free fluorophore ($[\text{M} + \text{H}]^+ = 1053.37$) and one corresponding to 4-aminobenzyl alcohol ($[\text{M} + \text{H}]^+ = 124.076$) (Figure S24). Moreover, new bands, consistent with the NTR-promoted self-immolative ether bond cleavage, were observed in the HPLC chromatogram (Figure S25). It was also observed that the presence of potential biological interferants had little adverse effects on the

cleavage process. Species tested in this regard included metal ions (Na^+ , K^+ , Ca^{2+} , and Mg^{2+}), amino acids (cysteine, serine, homocysteine, glutamic acid, arginine, and glutathione), NADH, DTT glucose, vitamin C, vitamin B₆, and H₂O₂ (Figure 4A). We also monitored the evolution of the NTR-mediated fluorescence emission intensity increase in the case of fol-BODIPY (cf. Figures 4C and S26). Saturation was reached within 25 min following initial exposure to NTR (1 $\mu\text{g}/\text{mL}$) in the presence of NADH (200 μM) at 37 °C. We also examined the reactivity of fol-BODIPY toward NTR as a function of pH. As shown in Figure 4D, the fluorescence emission intensity at $\lambda_{\text{em}} = 730$ nm recorded in the presence of NTR (1 $\mu\text{g}/\text{mL}$) was near maximal at pH 7. Good plasma stability was also seen for fol-BODIPY over the course of 48 h (Figure S27). Taken in aggregate, these predicative studies provide support for the notion that fol-BODIPY could serve as a useful probe for hypoxic cancer cells and hypoxic tumor microenvironments.

***In Vitro* Probe Activation and Imaging of Hypoxic CT-26 Cells.** Cytotoxicity is a major issue to consider in the context of biological probe development. Cell proliferation studies [(3-(4,5-dimethylthiazol-2-yl)-2,5-diphenyl tetrazolium bromide (MTT) assays] were thus carried out in the CT26

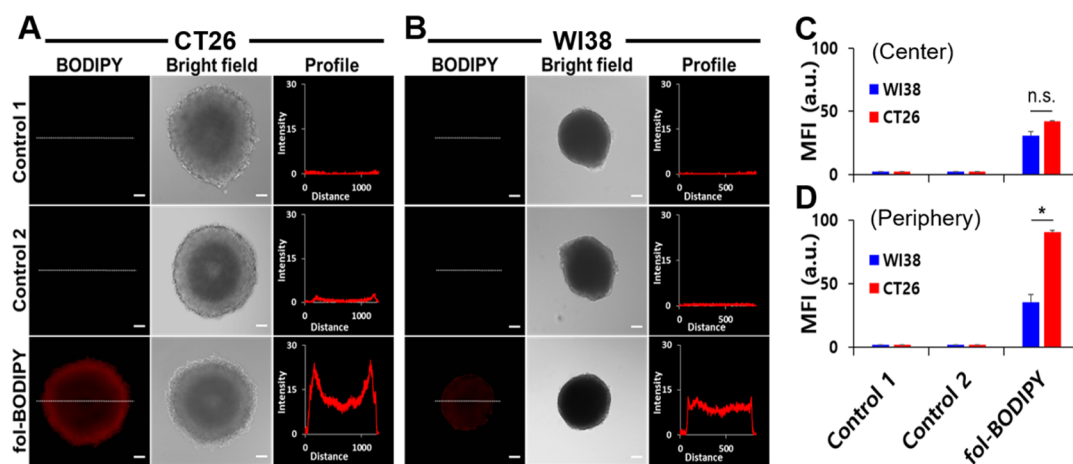


Figure 6. *In vitro* fluorescence imaging of cell spheroids with fol-BODIPY. Representative fluorescence ($E_x/E_m = 685/730$ nm) and bright-field images of tumor CT26 (A) and normal WI38 (B) cell spheroids incubated under culture conditions with fol-BODIPY or controls 1 and 2 (10 μ M, each) and corresponding quantitative comparison of the MFI measured in ROIs (regions of interest) of the spheroid center (C) and periphery (D). Two independent experiments were performed, and the error bars represent the standard deviation (nonpaired Student's *t*-test). Scale bar: 100 μ m. **p* < 0.05.

and WI38 cell lines using fol-BODIPY and control 1. Gratifyingly, both probes proved essentially nontoxic with $\geq 90\%$ cell viability being seen after incubation with 0–50 μ M for 24 h (Figures S28).

As noted above, the fol-BODIPY probe comprises a folate tumor-targeting element. Therefore, we expected it to target selectively folate receptor-enriched CT26 cells relative to folate receptor-negative cell lines, such as WI38. After confirming that hypoxia was maintained in the 1% oxygen incubator used for these studies by Western blot analysis of hypoxia-inducible factor-1 α protein (HIF-1 α) as a hypoxia marker (Figure S29), we incubated CT-26 cells with fol-BODIPY and, separately, control probes 1 and 2 (5 μ M in all cases) under both normoxic and hypoxic (1% oxygen) conditions. The cellular uptake of fol-BODIPY and controls was confirmed using confocal laser scanning microscopy (CLSM) to affect live cell imaging. As shown in Figure 5A, a strong fluorescence was seen in CT26 cells 15 min post-incubation with fol-BODIPY (10 μ M) under hypoxic conditions; the effect was greater than under normoxic conditions (Figure 5B). The relative normoxia–hypoxia fluorescent intensity was determined using ImageJ software (Java, Maryland, USA) in CT26 cells treated with either control 1, control 2, or fol-BODIPY (Figure 5C). These studies revealed very high normoxia–hypoxia fluorescence intensity ratios in the case of fol-BODIPY. Further evidence of selective hypoxic cell imaging in the case of CT26 cells came from live cell fluorescence-activated cell sorting (FACS) studies, which revealed that fol-BODIPY gives rise to a high level of fluorescence under these simulated hypoxic conditions (Figure 5C,D). In contrast, only a subtle fluorescence difference was seen under otherwise identical experiment conditions in the case of WI38 cells (Figure S30). Little or no fluorescence intensity increase or hypoxic versus normoxic differentiation was seen in the case of controls 1 and 2. Adventitious reduction of fol-BODIPY in the case of normoxic cells could serve as a potential limitation. However, in nitroaromatic compounds with suitable reduction potentials (approximately –330 to –450 mV), the first radical anions formed by one-electron addition can be efficiently scavenged by molecular oxygen. As a result, the fully cleaved daughter products are only observed in appreciably hypoxic

cells.^{54,55} We thus believe that fol-BODIPY may be used to distinguish effectively hypoxic cells from normoxic cells.

CT26 cells were also incubated for different times (2, 4, 6, 8, and 24 h) under the hypoxic conditions (1% oxygen) before being treated with either fol-BODIPY or control 1 (1 μ M in each) for 15 min prior to analysis (Figure S31). In contrast to what was seen for control 1, the fluorescence intensity of fol-BODIPY was found to increase as a function of pre-incubation time (Figure S32). These findings are rationalized in terms of the effectiveness of hypoxia increasing as a function of time, which translates into a more reducing environment leading to greater activation of fol-BODIPY.

To test the effectiveness of fol-BODIPY in hypoxic tumor microenvironments, fluorescence microscopic images of folate receptor-positive^{56,57} tumor CT26 (Figure 6A) and folate receptor-negative^{58,59} normal WI38 cells (Figure 6B) in 3D spheroid culture condition were recorded after incubating with fol-BODIPY or control 1 or 2 (10 μ M). In both the spheroid center and periphery, higher fluorescence signals were observed only in the fol-BODIPY group, while only a minimal fluorescence signature was seen in the case of control 1 and 2 groups. There was a nonsignificant difference in the spheroid center between CT26 and WI38 cells (Figure 6C; 52 ± 1 vs 41 ± 4 , *p* = 0.25), indicating that fol-BODIPY can travel intercellularly to the spheroid center, where it is then presumably reduced via hypoxia to produce a fluorescent signal. Enhanced (2.5-fold higher) mean fluorescence intensity (MFI) in the fol-BODIPY group was observed in the folate receptor-positive CT26 tumor spheroid periphery compared to the normal WI-38 cells (Figure 6D; 91 ± 2 vs 35 ± 6 ; *p* = 0.031). This difference is ascribed to folate receptor-mediated intracellular uptake and accumulation of fol-BODIPY as it encounters cells in the spheroid periphery, an effect that is expected to be enhanced in the case of CT26-derived spheroids. In the CT26 tumor spheroids incubated with fol-BODIPY, higher fluorescent MFI was observed in the tumor periphery than in the tumor core region (center) (91 ± 2 vs 52 ± 1 ; *p* = 0.043). This finding is consistent with fol-BODIPY accumulating relatively well in the peripheral region notwithstanding the fact that the cores of these tumor models are more hypoxic than the peripheral regions.^{60,61} In other words for

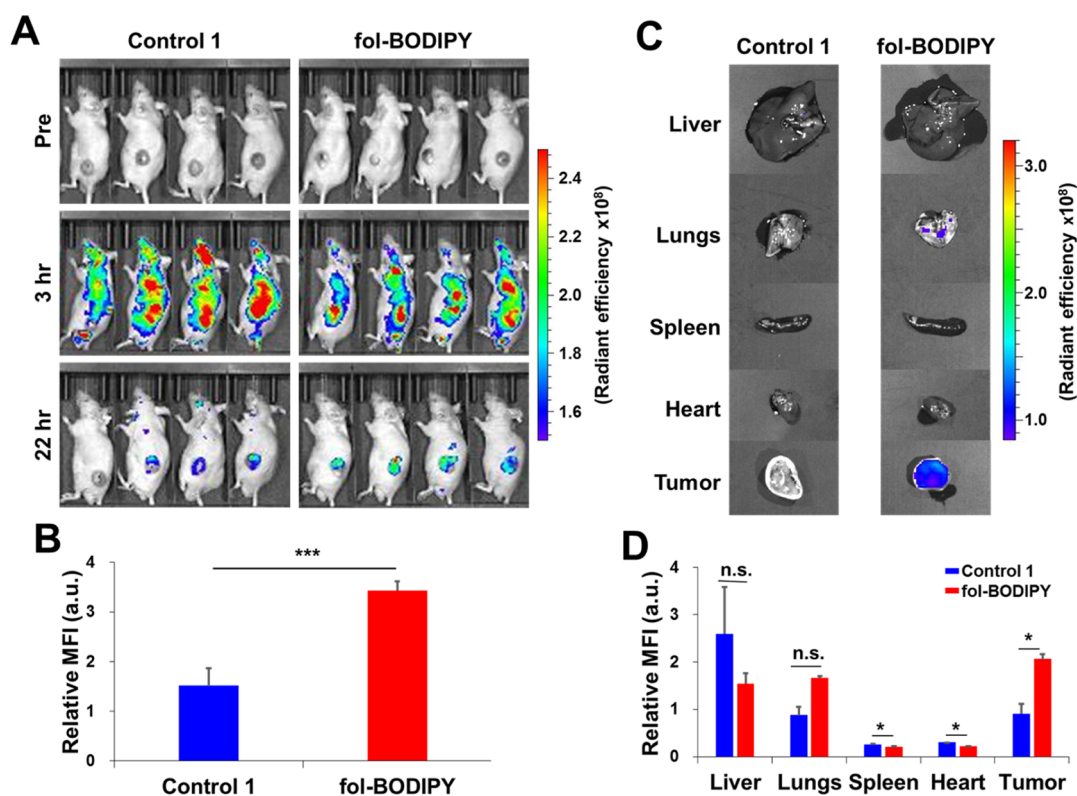


Figure 7. Tumor detection *in vivo* carried out by means of fluorescence imaging with fol-BODIPY. (A) Time-dependent *in vivo* optical imaging of xenograft CT26 tumor-bearing mice following intravenous injection of fol-BODIPY or control 1 (1 mM each, 100 μ L) and (B) corresponding quantitative comparison of the MFI obtained in the tumor region of CT26 tumor-bearing mice ($n = 5$) at 22 h post-injection (nonpaired Student's *t*-test). (C) Representative *ex vivo* fluorescence images obtained from several organs including the liver, lungs, spleen, heart, and tumor, extracted after final *in vivo* imaging at 22 h, for the fol-BODIPY group compared with the control 1 group. (D) Corresponding comparison of the relative mean fluorescence intensity (MFI) measured in tumor tissues ($n = 3$), and error bars are the standard deviations (nonpaired Student's *t*-test). * $p < 0.05$ and *** $p < 0.001$.

spheroids, it is predicted that the nature of the cells plays a dominant role in determining signal intensity. Support for this conclusion comes from the finding that a relatively weak signal is seen in the case of the folate receptor-negative WI38 spheroids.

In Vivo and Ex Vivo Fluorescence Imaging of the Hypoxic CT26 Tumor-Bearing Mouse Model Using fol-BODIPY. The potential use of fol-BODIPY as a specific tumor-targeting fluorescent probe for bio-imaging was further investigated by monitoring the fluorescence emission in xenograft tumor models and in different organs *in vivo*. Toward this end, CT26 hypoxic tumor-bearing nude mice were injected with fol-BODIPY, control 1, or PBS at the tumor site. *In vivo* images were obtained at various times. A readily discernible NIR fluorescence was seen immediately after injection of the probe (Figure S33A). The NIR fluorescence initially increased with time before eventually fading. At 25 h, the fluorescence intensity seen with fol-BODIPY in the tumor region was ~ 2.4 -fold higher than that produced by control 1 (Figure S33B). The folate subunit provides a degree of tumor targeting, leading to preferential uptake in tumor cells. This, in turn, allows a readily distinguishable fluorescent signal to be observed for fol-BODIPY. Importantly, these data serve to underscore the fact that fol-BODIPY is more effective in detecting hypoxia than controls. fol-BODIPY and control 1 in PBS buffer were also administered to CT26 cell-inoculated xenograft mice via intravenous injection. After 22 h, evidence of accumulation

of fol-BODIPY was seen based on the observation of an enhanced tumor-specific fluorescence emission (Figure 7A). Quantitative analyses revealed that the fluorescence intensity at the tumor site was approximately 2-fold higher in the case of fol-BODIPY as compared to control 1 (Figure 7C). After sacrifice, organs and tumor tissues were harvested from the mice and their respective fluorescence intensities were compared. Appreciable fluorescence was observed only in the solid tumors obtained from the animals treated with fol-BODIPY; no *ex vivo* fluorescence was detected in the heart, body, liver, lung, and spleen (Figure 7B, left side), unlike the results observed in the corresponding studies carried out with control 1 (Figure 7B). Quantification of the data revealed a 2.5-fold higher fluorescence intensity for fol-BODIPY at the tumor region than in the case of control 1 (Figure 7D). On the basis of these combined findings, we propose that fol-BODIPY may be used to target hypoxic tumors effectively without inducing acute side effects in other major organs, such as the liver, lungs, spleen, and heart. No adverse reactions were observed during or after imaging with our probes, nor was seen appreciable animal weight loss. We thus believe that fol-BODIPY constitutes an attractive hypoxia-responsive fluorochrome that permits effective NIR tumor imaging.

CONCLUSIONS

The cancer cell-targeting hypoxia-activatable fol-BODIPY probe was designed based on DFT-optimized quantum chemical calculations to permit cancer cell labeling and

tumor imaging. The fluorescence emission of **fol-BODIPY** proved responsive to hypoxia; it was roughly 20-fold more intense under hypoxic conditions when activated by exposure to NTR than two control probes **1** and **2**. Moreover, a fast response time (<5 min) and ultra-sensitivity (detection limit of ca. 1.5 ng/mL) were seen. *In vitro* CLSM and FACS studies revealed that compared with the control probes, **fol-BODIPY** is more easily taken up by folate receptor-positive CT26 cancer cells and produces a greater NIR signal under hypoxic conditions. These imaging benefits were recapitulated in 3D-cultured hypoxia-mimicking spheroid cells. *In vivo* studies, involving CT26 cell-derived mouse xenografts, served to confirm that relative to control **1**, which lacks a folate-based tumor-targeting moiety, **fol-BODIPY** selectively accumulates in the solid tumor region after tail vein injection, giving rise to maximally enhanced fluorescence intensity within 1 day. This tumor-targeting ability and the observation of specific activation in hypoxic tumor regions leads us to suggest that **fol-BODIPY** is a promising fluorescence “off–on” probe that could be used in potential applications, such as initial diagnosis of surgery, where the fluorescence-guided image detection of tumor tissue would be beneficial.

EXPERIMENTAL SECTION

Materials and Instrumentation. Commercial analytical grade chemicals were purchased and used without further purification. Further details including the chemical synthesis of compounds are provided in the [Supporting Information](#).

Synthesis of Control 1. A dimethylformamide (DMF) solution (5 mL) of compound **4** (Scheme S1, 643.5 mg, 1.0 mmol) and K_2CO_3 (276.42 mg, 2 mmol) were stirred at 0 °C under a nitrogen atmosphere for 10 min. Then, 4-nitrobenzylbromide (324 mg, 1.5 mmol) in 3 mL of DMF was added slowly to the reaction mixture, which was stirred at room temperature (RT) overnight. The reaction mixture was diluted with water and extracted with EtOAc. After collecting the organic layer and removing the bulk of the solvent under reduced pressure, the crude compound was purified by silica gel column chromatography using ethyl acetate/hexanes (EtOAc/Hex) (1:2) as the eluent; this afforded 710 mg (91.19%) of control **1**. 1H NMR (400 MHz, DMSO- d_6): δ 8.29 (d, J = 6.4, 2H); 8.17 (m, 8H); 7.77 (d, J = 5.28, 2H); 7.60 (m, 2H); 7.53 (d, J = 4.44, 2H); 7.48 (m, 6H); 7.24 (d, J = 4.8, 2H); 7.12 (d, J = 8.36, 2H); 5.42 (s, 1H); 4.83 (s, 1H); 1.46 (s, 9H). ^{13}C NMR (100 MHz, DMSO- d_6): 170.30, 161.03, 160.89, 157.89, 157.77, 154.40, 154.26, 147.56, 145.01, 144.89, 142.61, 133.39, 132.25, 132.16, 130.02, 129.57, 129.36, 129.13, 128.81, 128.76, 124.18, 124.13, 124.12, 120.28, 116.29, 116.00, 115.67, 115.35 ppm. ESI HR-MS m/z ($M + Na$): calcd 801.26; found, 801.2667.

Synthesis of fol-BODIPY. Compound **6a** (Scheme S1) was synthesized from 4-hydroxychalconone (purchased commercially) in six consecutive steps as detailed in the [Supporting Information](#). Briefly, a mixture of compound **6a** (145 mg, 0.2 mmol) and *N*-(3-dimethyl-aminopropyl)-*N'*-ethylcarbodiimide hydrochloride (77 mg, 0.4 mmol) was dissolved in anhydrous dimethyl sulfoxide (DMSO, 2 mL) and stirred at RT for 3 h under a N_2 atmosphere. The solution was extracted with dichloromethane (DCM) (50 mL) and 0.5 M HCl (50 mL). The organic phases were washed with 0.5 M HCl brine and dried over anhydrous Na_2SO_4 , filtered, and evaporated to dryness on a rotary evaporator, while the temperature of the water bath was kept below 40 °C. The solid material obtained in this way and folate ethylenediamine (compound **2**) (87 mg, 0.18 mmol) were then dissolved in 2 mL of anhydrous DMSO and stirred at RT for 18 h under a N_2 atmosphere. The volatiles were removed by means of a short path distillation column under reduced pressure at RT. The crude product obtained in this way was partitioned between DCM (50 mL) and 1 M Na_2CO_3 (50 mL). The aqueous phase was extracted using DCM (3 \times 30 mL). The organic layers were washed

with brine and dried over anhydrous Na_2SO_4 , filtered, and evaporated to dryness under reduced pressure. The residue was washed with 20% acetone in ether, acetone, and ether. The product **fol-BODIPY** was obtained as a dark green solid (175 mg, 73.5%). 1H nuclear magnetic resonance (NMR) (400 MHz, DMSO- d_6): δ 11.43 (s, 1H); 8.65 (d, J = 8.68, 1H); 8.30–8.21 (m, 2H); 8.19–8.1 (m, 5H); 8.08–8.2 (m, 3H); 7.83 (d, J = 5.76, 2H); 7.78–7.73 (m, 3H); 7.69–7.63 (m, 4H); 7.55–7.46 (m, 5H); 7.47 (d, J = 6.44, 1H); 7.26–7.22 (m, 2H); 7.17 (d, J = 8.92, 2H); 6.94 (d, J = 6.56, 2H), 6.63 (s, 2H); 5.44 (s, 2H); 4.63 (t, J = 5.6, 2H); 4.49 (d, J = 6.2, 2H); 4.30 (s, 1H); 3.34 (m, 2H); 3.08 (d, J = 11.76, 2H); 2.40 (d, J = 7.0, 2H); 2.28 (d, J = 6.64, 2H). ^{13}C NMR (100 MHz, DMSO- d_6): 180.72, 172.62, 172.50, 172.30, 172.23, 166.90, 154.21, 151.19, 149.07, 148.95, 144.93, 144.80, 133.68, 132.30, 132.05, 129.51, 129.02, 128.78, 128.72, 128.68, 128.59, 128.48, 128.22, 124.08, 123.98, 121.72, 120.13, 116.26, 115.47, 115.65, 68.72, 67.29, 65.35, 53.62, 46.26, 38.79, 34.56, 32.43 ppm. Electrospray ionization (ESI) high-resolution mass spectrometry (HR-MS) $[M + Na]^+$: calcd 1210.40; found, 1210.405. The purity of **fol-BODIPY** was confirmed as 98.7% by HPLC analysis.

Synthesis of Control 2. Control 2 (yield: 78.25%) was prepared using a procedure analogous to that used to prepare **fol-BODIPY** except for starting with compound **6b** (Scheme S1). 1H NMR (400 MHz, DMSO- d_6): δ 8.07 (d, J = 7.28, 4H); 8.00 (m, 5H); 7.56 (m, 5H); 7.50 (m, 8H); 7.38 (m, 4H); 7.28 (d, J = 8.4, 2H); 7.12 (d, J = 8.16, 2H); 5.24 (s, 2H); 4.78 (m, 1H); 4.48 (s, 2H); 3.17 (s, 2H); 2.89 (s, 4H); 2.73 (s, 4H). ^{13}C NMR (100 MHz, DMSO- d_6): 162.34, 160.28, 158.15, 157.84, 149.38, 147.91, 140.44, 136.71, 133.44, 133.33, 128.63, 128.58, 128.52, 128.28, 128.19, 128.02, 127.85, 124.12, 123.52, 118.81, 115.83, 115.63, 114.82, 69.56, 60.22, 48.58, 45.32, 35.80, 30.78, 20.79 ppm. ESI HR-MS m/z [$M + H$] $^+$: calcd 1142.42; found, 1142.4102.

Absorption and Fluorescence Studies. Fluorescence and UV–vis spectra were recorded using a spectrophotometer (S-3100; Scinco, Seoul, Korea) in a 1 cm standard quartz cell and a UV-1800 spectrophotometer (Scinco), respectively. NTR from *Escherichia coli* was used in our experiments. Stock solutions of various analytes (NADH, KCl, $CaCl_2$, $MgCl_2$, glucose, vitamin C, 1 mM vitamin B_6 , HSA, H_2O_2 , $\cdot OH$, glutamic acid, arginine, serine, glutathione, cysteine, homocysteine, and DTT) were prepared using double-distilled water. A stock solution of **fol-BODIPY** (20 μM) was prepared using Dulbecco's modified Eagle's medium (DMEM) containing 10% fetal bovine serum (FBS) (pH 7.4) and 0.2% DMSO. The fluorescence spectra were obtained at excitation wavelengths under 685 nm using a 5 nm slit width. The fluorescence changes of **fol-BODIPY** (5.0 μM) were recorded in the presence of increasing concentrations of NTR (0–1 $\mu g/mL$) in DMEM with 10% FBS (pH 7.4) and 0.2% DMSO. For these studies, **fol-BODIPY** was incubated with NTR for 30 min at 37 °C. The fluorescence quantum yield of **fol-BODIPY** was measured in the presence and absence of NTR in the cell medium (pH 7.4).

Quantum Chemical Calculations. Quantum chemical calculations were carried out by using a quantum chemical calculation program (ORCA 4.0.1, Max-Planck Institute, Berlin, Germany).⁶² The structures were optimized using the BP86 exchange correlation DFT^{63,64} in conjunction with a Karlsruhe split valence polarization def2-SVP basis set^{65,66} for all atoms. Due to the large system size, a medium-sized split valence basis set was used; it proved adequate to support our experimental predictions. This method and basis set combination has previously been used by us and found to give rise to acceptable predictions of geometric and electronic structure.^{51–53}

NTR Detection Assay Using HPLC. HPLC was performed using an HPLC system (YL9100, Youngin, Seoul, South Korea) with a Sunfire C18 column (4.6 mm \times 150 mm, 5 μm , Waters, Massachusetts, USA). The conditions were as follows: volume ratio of acetonitrile/ H_2O = 100:0 (0 min) to 60:40 (20 min); flow rate 1 mL/min; and UV detection at ≤ 254 nm.

Linear Range and Detection Limit. The detection limit of the **fol-BODIPY** probe toward NTR was calculated based on fluorescence spectroscopic titrations. The fluorescence emission

spectrum of fol-BODIPY (2 μ M) was measured 10 times. The standard deviation of the blank solution was also measured. The fluorescence intensity ($\lambda_{em} = 730$ nm) of the probe was plotted versus the concentrations of NTR. The detection limit was calculated using the following equation: detection limit = $3\sigma/k$, where σ is the standard deviation of the blank measurement and k is the slope between the fluorescence intensity versus the NTR concentration.

Determination of the Fluorescence Quantum Yield. The fluorescence quantum yield of fol-BODIPY in the presence and absence of NTR was determined in PBS buffer (10 mM, pH 7.4) using BF₂-chelated tetra-arylazadipyromethene ($\Phi_X = 0.36$) as a standard. The fluorescence quantum yield was calculated using the following equation: $\Phi_S = \Phi_X (A_S F_S / A_X F_X)$, where Φ_X is the standard fluorescence quantum yield, Φ_S is the sample fluorescence quantum yield, A_S and A_X are the absorbance of the sample and the reference, respectively, at the same excitation wavelength, and F_S and F_X are the corresponding relative integrated fluorescence intensities.

Cells. The CT26 (mouse colon cancer; folate receptor-positive) cell line was kindly provided by Y. S. Gho (POSTECH, Korea) and cultured in minimum essential media (MEM, Gibco, Grand Island, NY, USA) containing 10% FBS (Gibco) and 1% antibiotic-antimycotic (Gibco). The WI-38 (human lung fibroblast; folate receptor-negative) cell line was obtained from the American Type Culture Collection (ATCC, Rockville, MD, USA). The WI-38 cells were maintained in Eagle's minimum essential medium (EMEM, ATCC) supplemented with 10% FBS and 1% antibiotic-antimycotic at 37 °C in a humidified atmosphere containing 5% CO₂.

In Vitro Cell Imaging. Cells were seeded at a density of 2×10^4 cells/well in eight-well plates (Ibidi, Martinsried, Germany) at 37 °C in a humidified incubator and kept overnight. The next day, the cells were transferred to a hypoxia (1% O₂) incubator chamber (STEMCELL Technologies, Inc., Vancouver, BC, Canada) or kept under normoxic conditions for 8 h and then incubated either with 5 μ M fol-BODIPY or a control probe for 15 min. Fluorescence images were acquired using a confocal laser scanning fluorescence microscope (LSM710, Carl Zeiss, Oberkochen, Germany) equipped with a BODIPY filter set. For fluorescence imaging of spheroids, cells were seeded at a density of 2×10^4 cells/well in ultra-low attachment 96-well plates (Corning Costar, New York, USA) and grown for 3 days. The spheroids that formed were then treated with 10 μ M fol-BODIPY or the control probes 1 or 2 for 24 h. Fluorescence images were acquired using an Olympus IX81 microscope equipped with a Cy7 filter set.

Cell Viability. The folate receptor-positive (CT26) and -negative (WI-38) cell lines were used to evaluate the cytotoxicity of fol-BODIPY and the control probes. Cells were seeded at a density of 10,000 cells/well in 96-well plates and grown overnight at 37 °C in an incubator with 5% CO₂. The next day, the cells were incubated with different concentrations of fol-BODIPY and control 1 for 24 h before being subject to exchange with a fresh culture medium containing 10% MTT assay (5 mg/ml in PBS) solution and incubating for an additional 2 h at 37 °C. Subsequently, the medium was removed and the cells were dissolved in 100 μ L of DMSO. The absorbance was measured using a microplate reader (XMark, Bio-Rad, Berkeley, CA, USA) at 570 nm.

Flow Cytometric Analyses. CT26 and WI-38 cells were seeded at a density of 1.5×10^5 cells/well in six-well plates, grown for 20 h, and then pre-incubated for 8 h under hypoxic or normoxic conditions prior to incubation with fol-BODIPY or controls 1 or 2. After incubation for 15 min, the cells were gently scraped, suspended in PBS (Gibco), and transferred to flow cytometry tubes. Subsequently, the cells were analyzed using a flow cytometer (Attune NxT, Thermo Fisher) for red RL2 fluorescence (638 nm excitation, 720/30 nm emission). All analyses were carried out in triplicate using at least 10,000 cells.

In Vivo and Ex Vivo Animal Imaging. All animal experiments were performed according to protocols approved by the Institutional Animal Care and Use Committee of the Korean Basic Sciences Institute (KBSI-AEC-1803). A mouse tumor model was established by injecting CT26 cells (5×10^5 cells per mouse) subcutaneously into

the left flank region of 6 week-old male mice (Balb/c-nude), and the animals were split into two groups ($n = 3$ each group). Ten days after tumor inoculation, tumors reached an average diameter of 7 mm before injection. At this point, the fol-BODIPY or control 1 probe (2 mg/kg) dissolved in 2.5% DMSO (100 μ L) was intravenously administered via the tail vein, and *in vivo* fluorescence images were acquired at 3, 6, and 22 h post-intravenous (IV) injection of the probes using an optical imaging system (IVIS Spectrum, PerkinElmer). The fluorescence images were collected using an optical imaging system (IVIS Spectrum; $E_x/E_m = 675/740$ nm) equipped with a 30 nm bandpass filter. The animals were sacrificed 24 h post-IV injection, and several organs including the liver, lungs, spleen, heart, and tumor were sampled. Subsequently, *ex vivo* imaging was performed using the same imaging system.

■ ASSOCIATED CONTENT

Supporting Information

The Supporting Information is available free of charge at <https://pubs.acs.org/doi/10.1021/acs.jmedchem.0c02162>.

Materials and methods; ¹H NMR, ¹³C NMR, HR-MS ESI, HPLC chromatogram, optimized structure and absorption spectrum, UV absorption spectrum, fluorescence emission spectra, detection limit, HPLC profiles, stability test, cell cytotoxicity, western blot analysis, flow cytometric analysis, and CLSM images; and spectroscopic data of compounds (PDF)

Molecular formula strings (CSV)

■ AUTHOR INFORMATION

Corresponding Authors

Jonathan L. Sessler – Department of Chemistry, The University of Texas at Austin, Austin, Texas 78712-1224, United States; orcid.org/0000-0002-9576-1325; Email: seessler@cm.utexas.edu

Kwan Soo Hong – Research Center for Bioconvergence Analysis, Korea Basic Science Institute, Cheongju 28119, Republic of Korea; Graduate School of Analytical Science and Technology, Chungnam National University, Daejeon 34134, Republic of Korea; orcid.org/0000-0003-4342-5183; Email: kshong@kbsi.re.kr

Authors

Sanu Karan – Research Center for Bioconvergence Analysis, Korea Basic Science Institute, Cheongju 28119, Republic of Korea; Graduate School of Analytical Science and Technology, Chungnam National University, Daejeon 34134, Republic of Korea

Mi Young Cho – Research Center for Bioconvergence Analysis, Korea Basic Science Institute, Cheongju 28119, Republic of Korea

Hyunseung Lee – Research Center for Bioconvergence Analysis, Korea Basic Science Institute, Cheongju 28119, Republic of Korea

Hwunjae Lee – Research Center for Bioconvergence Analysis, Korea Basic Science Institute, Cheongju 28119, Republic of Korea

Hye Sun Park – Research Center for Bioconvergence Analysis, Korea Basic Science Institute, Cheongju 28119, Republic of Korea

Mahesh Sundararajan – Theoretical Chemistry Section, Bhabha Atomic Research Centre, Mumbai 400 085, India; orcid.org/0000-0002-1522-124X

Complete contact information is available at:

<https://pubs.acs.org/10.1021/acs.jmedchem.0c02162>

Author Contributions

S.K., M.Y.C., and H.L. equally contributed to this work. The manuscript was written through the contribution of all authors. All authors have given approval to the final version of the manuscript.

Notes

The authors declare no competing financial interest.

ACKNOWLEDGMENTS

This work was supported by the National Research Council of Science and Technology (NST) grant from the Korea government (MSIT) (K.S.H., CAP-18-02-KRIBB) and the National Research Foundation of Korea (NRF) grant funded by the Korea government (MSIT) (K.S.H., 2020R1A2C2012011). The work in Austin was supported by the Robert A. Welch Foundation (F-0018 to J.L.S.).

ABBREVIATIONS

BOC, *tert*-butoxycarbonyl; DCC, *N,N'*-dicyclohexylcarbodiimide; DCM, dichloromethane; DFT, density functional theory; DIEA, diisopropylethylamine; DMAP, 4-(*N,N*-dimethylamino)pyridine; DMF, dimethylformamide; DMSO, dimethyl sulfoxide; E_x , excitation; E_m , emission; fol, folate; FR- α , folate receptor; HIF-1 α/β , hypoxia-inducible factors; HOMO, highest occupied molecular orbital; HPLC, high-performance liquid chromatography; HRMS, high-resolution mass spectrometry; J , coupling constant (in NMR spectrometry); LUMO, lowest unoccupied molecular orbital; m/z , mass-to-charge ratio; MFI, mean fluorescence intensity; MS, mass spectrometry; NADH, reduced nicotinamide adenine dinucleotide; NHS, *N*-hydroxysuccinimide; NIR, near infrared; NMR, nuclear magnetic resonance; NTR, nitroreductase; OD, optical density; PBS, phosphate-buffered saline; PET, positron emission tomography; Ph, phenyl; *t*-Bu, *tert*-butyl; TFA, trifluoroacetic acid; TLC, thin-layer chromatography; UV, ultraviolet

REFERENCES

- (1) Gatenby, R. A.; Gillies, R. J. A microenvironmental model of carcinogenesis. *Nat. Rev. Cancer* **2008**, *8*, 56–61.
- (2) Contag, C. H. In vivo pathology: seeing with molecular specificity and cellular resolution in the living body. *Annu. Rev. Pathol.* **2007**, *2*, 277–305.
- (3) Vaupel, P.; Kallinowski, F.; Okunieff, P. Blood flow, oxygen and nutrient supply, and metabolic microenvironment of human tumors: a review. *Cancer Res.* **1989**, *49*, 6449–6465.
- (4) Harada, H.; Inoue, M.; Itasaka, S.; Hirota, K.; Morinibu, A.; Shinomiya, K.; Zeng, L.; Ou, G.; Zhu, Y.; Yoshimura, M.; Mckenna, W. G.; Muschel, R. J.; Hirakora, M. Cancer cells that survive radiation therapy acquire HIF-1 activity and translocate towards tumour blood vessels. *Nat. Commun.* **2012**, *3*, 783.
- (5) Hanahan, D.; Weinberg, R. A. The hallmarks of cancer. *Cell* **2000**, *100*, 57–70.
- (6) Schaible, B.; McClean, S.; Selfridge, A.; Broquet, A.; Asehnoune, K.; Taylor, C. T.; Schaffer, K. Hypoxia modulates infection of epithelial cells by *Pseudomonas aeruginosa*. *PLoS One* **2013**, *8*, No. e56491.
- (7) Nath, B.; Szabo, G. Hypoxia and hypoxia inducible factors: diverse roles in liver diseases. *Hepatology* **2012**, *55*, 622–633.
- (8) Semenza, G. L. Hypoxia-inducible factors in physiology and medicine. *Cell* **2012**, *148*, 399–408.
- (9) Taylor, C. T.; Colgan, S. P. Hypoxia and gastrointestinal disease. *J. Mol. Med.* **2007**, *85*, 1295–1300.

- (10) Chaudary, N.; Hill, R. P. Hypoxia and metastasis. *Clin. Cancer Res.* **2007**, *13*, 1947–1949.
- (11) Bristow, R. G.; Hill, R. P. Hypoxia, DNA repair and genetic instability. *Nat. Rev. Cancer* **2008**, *8*, 180–192.
- (12) Brahimi-Horn, M. C.; Chiche, J.; Pouyssegur, J. Hypoxia and cancer. *J. Mol. Med.* **2007**, *85*, 1301–1307.
- (13) Sun, X.; Niu, G.; Chan, N.; Shen, B.; Chen, X. Tumor hypoxia imaging. *Mol. Imag. Biol.* **2011**, *13*, 399–410.
- (14) Weissleder, R. Molecular imaging in cancer. *Science* **2006**, *312*, 1168–1171.
- (15) Lee, S.; Xie, J.; Chen, X. Activatable molecular probes for cancer imaging. *Curr. Top. Med. Chem.* **2010**, *10*, 1135–1144.
- (16) Ntziachristos, V. Going deeper than microscopy: the optical imaging frontier in biology. *Nat. Methods* **2010**, *7*, 603–614.
- (17) Whiteway, J.; Koziazar, P.; Veall, J.; Sandhu, N.; Kumar, P.; Hoecher, B.; Lambert, I. B. Oxygen-Insensitive Nitroreductases: Analysis of the Roles of *nfsA* and *nfsB* in Development of Resistance to 5-Nitrofuranyl Derivatives in *Escherichia coli*. *J. Bacteriol.* **1998**, *180*, 5529–5539.
- (18) Mason, R. P.; Holtzman, J. L. The role of catalytic superoxide formation in the O₂ inhibition of nitroreductase. *Biochem. Biophys. Res. Commun.* **1975**, *67*, 1267–1274.
- (19) Hodgkiss, R. J.; Jones, G. W.; Long, A.; Middleton, R. W.; Parrick, J.; Stratford, M. R. L.; Wardman, P.; Wilson, G. D. Fluorescent markers for hypoxic cells: a study of nitroaromatic compounds, with fluorescent heterocyclic side chains, that undergo bioreductive binding. *J. Med. Chem.* **1991**, *34*, 2268–2274.
- (20) Liu, Y.; Xu, Y.; Qian, X.; Liu, J.; Shen, L.; Li, J.; Zhang, Y. Novel fluorescent markers for hypoxic cells of naphthalimides with two heterocyclic side chains for bioreductive binding. *Bioorg. Med. Chem.* **2006**, *14*, 2935–2941.
- (21) Tanabe, K.; Hirata, N.; Harada, H.; Hiraoka, M.; Nishimoto, S.-i. Emission under hypoxia: one-electron reduction and fluorescence characteristics of an indolequinone-coumarin conjugate. *Chembiochem* **2008**, *9*, 426–432.
- (22) Sandhu, S.; Kydd, L.; Jaworski, J. Luminescent Probe Based Techniques for Hypoxia Imaging. *J. Nanomed. Res.* **2017**, *6*, 00160.
- (23) Chen, H.; Bi, Q.; Yao, Y.; Tan, N. Dimeric BODIPY-loaded liposomes for dual hypoxia marker imaging and activatable photodynamic therapy against tumors. *J. Mater. Chem. B* **2018**, *6*, 4351–4359.
- (24) Fleming, I. N.; Manavaki, R.; Blower, P. J.; West, C.; Williams, K. J.; Harris, A. L.; Domarkas, J.; Lord, S.; Baldry, C.; Gilbert, F. J. Imaging tumour hypoxia with positron emission tomography. *J. Cancer* **2015**, *112*, 238–250.
- (25) Gambhir, S. S. Molecular imaging of cancer with positron emission tomography. *Nat. Rev. Cancer* **2002**, *2*, 683–693.
- (26) Xu, K.; Wang, F.; Pan, X.; Liu, R.; Ma, J.; Kong, F.; Tang, B. High selectivity imaging of nitroreductase using a near-infrared fluorescence probe in hypoxic tumor. *Chem. Commun.* **2013**, *49*, 2554–2556.
- (27) Li, Y.; Sun, Y.; Li, J.; Su, Q.; Yuan, W.; Dai, Y.; Han, C.; Wang, Q.; Feng, W.; Li, F. Ultrasensitive near-infrared fluorescence-enhanced probe for in vivo nitroreductase imaging. *J. Am. Chem. Soc.* **2015**, *137*, 6407–6416.
- (28) Zheng, X.; Wang, X.; Mao, H.; Wu, W.; Liu, B.; Jiang, X. Hypoxia-specific ultrasensitive detection of tumours and cancer cells in vivo. *Nat. Commun.* **2015**, *6*, 5834.
- (29) Knox, H. J.; Hedhli, J.; Kim, T. W.; Khalili, K.; Dobrucki, L. W.; Chan, J. A bioreducible N-oxide-based probe for photoacoustic imaging of hypoxia. *Nat. Commun.* **2017**, *8*, 1794.
- (30) Zheng, J.; Shen, Y.; Xu, Z.; Yuan, Z.; He, Y.; Wei, C.; Er, M.; Yin, J.; Chen, H. Near-infrared off-on fluorescence probe activated by NTR for in vivo hypoxia imaging. *Biosens. Bioelectron.* **2018**, *119*, 141–148.
- (31) Gao, M.; Yu, F.; Lv, C.; Choo, J.; Chen, L. Fluorescent chemical probes for accurate tumor diagnosis and targeting therapy. *Chem. Soc. Rev.* **2017**, *46*, 2237–2271.

- (32) Kumar, R.; Kim, E.-J.; Han, J.; Lee, H.; Shin, W. S.; Kim, H. M.; Bhuniya, S.; Kim, J. S.; Hong, K. S. Hypoxia-directed and activated theranostic agent: Imaging and treatment of solid tumor. *Biomaterials* **2016**, *104*, 119–128.
- (33) Zhang, X.; Zhang, L.; Gao, M.; Wang, Y.; Chen, L. A near-infrared fluorescent probe for observing thionitrous acid-mediated hydrogen polysulfides formation and fluctuation in cells and in vivo under hypoxia stress. *J. Hazard. Mater.* **2020**, *396*, 122673.
- (34) Palma, A.; Alvarez, L. A.; Scholz, D.; Frimannsson, D. O.; Grossi, M.; Quinn, S. J.; O'Shea, D. F. Cellular uptake mediated off/on responsive near-infrared fluorescent nanoparticles. *J. Am. Chem. Soc.* **2011**, *133*, 19618–19621.
- (35) Batat, P.; Cantuel, M.; Jonusauskas, G.; Scarpantonio, L.; Palma, A.; O'Shea, D. F.; McClenaghan, N. D. BF₂-azadipyromethenes: probing the excited-state dynamics of a NIR fluorophore and photodynamic therapy agent. *J. Phys. Chem. A* **2011**, *115*, 14034–14039.
- (36) Tasiar, M.; O'Shea, D. F. BF₂-Chelated Tetraarylazadipyromethenes as NIR Fluorochromes. *Bioconjugate Chem.* **2010**, *21*, 1130–1133.
- (37) Shi, Z.; Han, X.; Hu, W.; Bai, H.; Peng, B.; Ji, L.; Fan, Q.; Li, L.; Huang, W. Bioapplications of small molecule Aza-BODIPY: from rational structural design to in vivo investigations. *Chem. Soc. Rev.* **2020**, *49*, 7533–7567.
- (38) Low, P. S.; Kularatne, S. A. Folate-targeted therapeutic and imaging agents for cancer. *Curr. Opin. Chem. Biol.* **2009**, *13*, 256–262.
- (39) Kalli, K. R.; Oberg, A. L.; Keeney, G. L.; Christianson, T. J. H.; Low, P. S.; Knutson, K. L.; Hartmann, L. C. Folate receptor alpha as a tumor target in epithelial ovarian cancer. *Gynecol. Oncol.* **2008**, *108*, 619–626.
- (40) Markert, S.; Lassmann, S.; Gabriel, B.; Klar, M.; Werner, M.; Gitsch, G.; Kratz, F.; Hasenburg, A. Alpha-folate receptor expression in epithelial ovarian carcinoma and non-neoplastic ovarian tissue. *Anticancer Res.* **2008**, *28*, 3567–3572.
- (41) D'Angelica, M.; Ammori, J.; Gonen, M.; Klimstra, D. S.; Low, P. S.; Murphy, L.; Weiser, M. R.; Paty, P. B.; Fong, Y.; Dematteo, R. P.; Allen, P.; Jarnagin, W. R.; Shia, J. Folate receptor- α expression in resectable hepatic colorectal cancer metastases: patterns and significance. *Mod. Pathol.* **2011**, *24*, 1221–1228.
- (42) Shia, J.; Klimstra, D. S.; Nitzkorski, J. R.; Low, P. S.; Gonen, M.; Landmann, R.; Weiser, M. R.; Franklin, W. A.; Prendergast, F. G.; Murphy, L.; Tang, L.; Guillem, J. G.; Wong, W. D.; Paty, P. B. Immunohistochemical expression of folate receptor α in colorectal carcinoma: patterns and biological significance. *Hum. Pathol.* **2008**, *39*, 498–505.
- (43) Kamaly, N.; Yameen, B.; Wu, J.; Farokhzad, O. C. Degradable Controlled-Release Polymers and Polymeric Nanoparticles: Mechanisms of Controlling Drug Release. *Chem. Rev.* **2016**, *116*, 2602–2663.
- (44) Yoo, H. S.; Park, T. G. Folate-receptor-targeted delivery of doxorubicin nano-aggregates stabilized by doxorubicin-PEG-folate conjugate. *J. Controlled Release* **2004**, *100*, 247–256.
- (45) Nakamura, J.; Nakajima, N.; Matsumura, K.; Hyon, S. H. Nanomedical platform for Drug Delivery. *J. Nanomed. Nanotechnol.* **2011**, *2*, 106–109.
- (46) Low, P. S.; Henne, W. A.; Doorneweerd, D. D. Discovery and Development of Folic-Acid-Based Receptor Targeting for Imaging and Therapy of Cancer and Inflammatory Diseases. *Chem. Res.* **2008**, *41*, 120–129.
- (47) Jaffar, M.; Williams, K. J.; Stratford, I. J. Bioreductive and gene therapy approaches to hypoxic diseases. *Adv. Drug Deliv. Rev.* **2001**, *53*, 217–228.
- (48) Murtagh, J.; Frimannsson, D. O.; O'Shea, D. F. Azide conjugatable and pH responsive near-infrared fluorescent imaging probes. *Org. Lett.* **2009**, *11*, 5386–5389.
- (49) Grossi, M.; Morgunova, M.; Cheung, S.; Scholz, D.; Conroy, E.; Terrile, M.; Panarella, A.; Simpson, J. C.; Gallagher, W. M.; O'Shea, D. F. Lysosome triggered near-infrared fluorescence imaging of cellular trafficking processes in real time. *Nat. Commun.* **2016**, *7*, 10855.
- (50) Trindade, A. F.; Frade, R. F. M.; Maçôas, E. M. S.; Graça, C.; Rodrigues, C. A. B.; Martinho, J. M. G.; Afonso, C. A. M. “Click and go”: simple and fast folic acid conjugation. *Org. Biomol. Chem.* **2014**, *12*, 3181–3190.
- (51) Sadhu, B.; Sundararajan, M.; Bandyopadhyay, T. Efficient Separation of Europium Over Americium Using Cucurbit-[5]-uril Supramolecule: A Relativistic DFT Based Investigation. *Inorg. Chem.* **2016**, *55*, 598–609.
- (52) Sundararajan, M.; Neese, F. Detailed QM/MM study of the electron paramagnetic resonance parameters of nitrosyl myoglobin. *J. Chem. Theory Comput.* **2012**, *8*, 563–574.
- (53) Sundararajan, M. Quantum chemical challenges for the binding of simple alkanes to supramolecular hosts. *J. Phys. Chem. B* **2013**, *117*, 13409–13417.
- (54) Laderoute, K.; Wardman, P.; Rauth, A. M. Molecular mechanisms for the hypoxiadependent activation of 3-amino-1,2,4-benzotriazine-1, 4-dioxide (SR 4233). *Biochem. Pharmacol.* **1988**, *37*, 1487–1495.
- (55) Wilson, W. R.; Van Zijl, P.; Denny, W. A. Bis-bioreductive agents as hypoxia-selective cytotoxins: nitracrine N-Oxide. *Int. J. Radiat. Oncol. Biol. Phys.* **1992**, *22*, 693–696.
- (56) Lee, M. H.; Kim, E.-J.; Lee, H.; Kim, H. M.; Chang, M. J.; Park, S. Y.; Hong, K. S.; Kim, J. S.; Sessler, J. L. Liposomal texaphyrin theranostics for metastatic liver cancer. *J. Am. Chem. Soc.* **2016**, *138*, 16380–16387.
- (57) Lee, J. Y.; Park, J. H.; Kim, S. W. Synthesis and evaluation of folate-immobilized 198Au@SiO₂ nanocomposite materials for the diagnosis of folate-receptor-overexpressed tumor. *Bull. Korean Chem. Soc.* **2016**, *37*, 219–225.
- (58) Lee, Y.-C.; Kim, M. I.; Woo, M.-A.; Park, H. G.; Han, J.-I. Effective peroxidase-like activity of a water-solubilized Fe-aminoclay for use in immunoassay. *Biosens. Bioelectron.* **2013**, *42*, 373–378.
- (59) Lee, R. J.; Low, P. S. Folate-mediated tumor cell targeting of liposome-entrapped doxorubicin in vitro. *Biochim. Biophys. Acta Biomembr.* **1995**, *1233*, 134–144.
- (60) Torok, S.; Rezel, M.; Kelemen, O.; Vegvari, A.; Watanabe, K.; Sugihara, Y.; Tisza, A.; Marton, T.; Kovacs, I.; Tóvári, J.; Laszlo, V.; Helbich, T. H.; Hegedus, B.; Klikovits, T.; Hoda, M. A.; Klepetko, W.; Paku, S.; Marko-Varga, G.; Dome, B. Limited tumor tissue drug penetration contributes to primary resistance against angiogenesis inhibitors. *Theranostics* **2017**, *7*, 400–412.
- (61) Macháľková, M.; Pavlatovská, B.; Micháľek, J.; Pruška, A.; Štěpka, K.; Nečasová, T.; Radaszkiewicz, K. A.; Kozubek, M.; Šmarda, J.; Preisler, J.; Navrátilová, J. Drug Penetration Analysis in 3D Cell Cultures Using Fiducial-Based Semiautomatic Coregistration of MALDI MSI and Immunofluorescence Images. *Anal. Chem.* **2019**, *91*, 13475–13484.
- (62) Neese, F. Software update: the ORCA program system, version 4.0. *Wiley Interdiscip. Rev.: Comput. Mol. Sci.* **2018**, *8*, No. e1327.
- (63) Becke, A. D. Density-functional exchange-energy approximation with correct asymptotic behavior. *Phys. Rev. A: At., Mol., Opt. Phys.* **1988**, *38*, 3098–3100.
- (64) Perdew, J. P. Density-functional approximation for the correlation energy of the inhomogeneous electron gas. *Phys. Rev. B: Condens. Matter Mater. Phys.* **1986**, *33*, 8822–8824.
- (65) Schäfer, A.; Huber, C.; Ahlrichs, R. Fully optimized contracted Gaussian basis sets of triple zeta valence quality for atoms Li to Kr. *J. Chem. Phys.* **1994**, *100*, 5829.
- (66) Weigend, F.; Ahlrichs, R. Balanced basis sets of split valence, triple zeta valence and quadruple zeta valence quality for H to Rn: Design and assessment of accuracy. *Phys. Chem. Chem. Phys.* **2005**, *7*, 3297–3305.